




# How well does MPAS simulate the West African Monsoon?

LAOUALI I TANIMOUNE<sup>1,\*</sup> , BABATUNDE J ABIODUN<sup>2</sup>, NIMON POWWEROU<sup>1</sup>, HARALD KUNSTMANN<sup>3</sup>, GERHARD SMIATEK<sup>3</sup>, VINCENT O AJAYI<sup>1</sup> and IBRAH S SANDA<sup>4</sup>

<sup>1</sup>West African Science Service Center on Climate Change and Adapted Land Use (WASCAL) Graduate Research Program, Federal University of Technology Akure, Akure, Nigeria.

<sup>2</sup>Climate Systems Analysis Group, Department of Environmental and Geographical Science, University of Cape Town, Cape Town, South Africa.

<sup>3</sup>Institute of Meteorology and Climate Research (IMK-IFU), Karlsruhe Institute of Technology, Kreuzeckbahnstr. 19, 82467 Garmisch-Partenkirchen, Germany.

<sup>4</sup>Centre Regional AGRHYMET, Niamey, Niger.

\*Corresponding author. e-mail: [ibrahimlawali2060@gmail.com](mailto:ibrahimlawali2060@gmail.com)

MS received 2 March 2023; revised 24 May 2023; accepted 8 October 2023

The West African Monsoon (WAM) system plays a crucial role in the West African climate system because it transports moisture from the Atlantic Ocean into the subcontinent in summer. This study evaluates the capability of the Model for Prediction Across Scales-Atmosphere (MPAS-A) to simulate the characteristic reproduce the WAM system and the associated rainfall-producing features. The MPAS model was used to perform a 30-year global climate simulation (1981–2010) at a regular grid (uniform resolution of 60 km). The simulation was initialized with the Climate Forecast System Reanalysis (CSFR) dataset. The results showed that MPAS simulate well the rainfall pattern over West Africa and reproduces the different phases of the monsoon dynamics system (i.e., the northward progression, the peak period, and the southward retreat). The model also reasonably replicates the pattern of the zonal components of wind and the vertical velocity. However, MPAS underestimates the orographic rainfall over the Guinea Coast, Jos Plateau, and Mount Cameroon. It also underestimates the vertical velocity and zonal wind magnitudes over the region. In addition, the model features a weaker temperature gradient than in the reanalysis. Understanding and correcting the sources of these model biases will enhance the suitability of MPAS for weather and seasonal forecasts over West Africa.

**Keywords.** Atmospheric; meteorology; MPAS-atmosphere; West Africa; monsoon.

## 1. Introduction

The monsoon is a global-scale circulation that is dominated by a seasonal reversal of winds originating from the difference in heating between land and Ocean (Sylla *et al.* 2009). The West African

Monsoon (WAM), a branch of the global monsoon, plays a crucial role in the climate of West Africa (WA). It modulates the seasonal change in circulation over WA and controls the spatial distribution of the temperature and precipitation over the region (Nicholson 2009). Two seasonal winds

characterize the WAM system: the north-easterly wind, which blows dry cold air to the region in winter; and the south-westerly wind, which brings moist warm air over the region in summer (Krishnamurthy and Ajayamohan 2010). The south-westerly flow transports moisture from the Atlantic Ocean to WA and causes seasonal rainfall over the subcontinent. Seasonal rainfall is essential for millions of West African people, whose cultures and lifestyles depend on the behaviour of the monsoon rains and the associated growing season (Sivakumar *et al.* 2014). In addition, given that rainfed agriculture is the mainstay of the economies of most West African countries, variations in WAM rainfall often devastate socio-economic activities and food security in WA (Omosho and Abiodun 2007). Hence, to minimize the devastating impacts of monsoon rainfall variability in WA, there is a need for improved seasonal prediction of the WAM and its associated rainfall. The WAM system includes a multitude of atmospheric features that interact in a complex way to generate rainfall over WA. These atmospheric features include the heat low, African easterly jet (AEJ), African easterly waves (AEWs), and mesoscale convective systems (MCSs) (Nicholson 2009). For example, during summer, the heat low induces maximum heating over the continent, resulting in a temperature gradient between the West African subcontinent and the Atlantic Ocean. This temperature gradient drives the southwest monsoon flow from the ocean into the continent (Sultan and Janicot 2003; Caniaux *et al.* 2011). The temperature gradient also induces the AEJ due to the thermal wind effect, and when the AEJ becomes unstable, it generates AEWs (Grist and Nicholson 2001). The low-level convergence associated with AEWs lifts the warm moist southwest monsoon flow to the level of free convection, thereby initiating thunderstorms and mesoscale convective systems that produce heavy rainfall and account for more than 75% of the rainfall over WA (Hagos and Cook 2007). Therefore, for a model to correctly simulate rainfall characteristics over WA, it must reproduce all these atmospheric systems and their complex interactions (Abiodun *et al.* 2010). Hence, understanding how contemporary climate models link West African precipitation with these atmospheric features is essential for improving the seasonal prediction over this subcontinent.

Several studies have discussed the strengths and weaknesses of global climate models (GCMs) when it comes to simulating atmospheric systems and

rainfall over WA (Cook and Vizy 2006; Hourdin *et al.* 2010; Xue *et al.* 2010; Sylla *et al.* 2012, 2013; Matte *et al.* 2017; Akinsanola *et al.* 2018; Ajibola *et al.* 2020; Chagnaud *et al.* 2020). For instance, by applying the 5th generation European Centre Hamburg general circulation model (ECHAM5) over WA, Sylla *et al.* (2012) showed that the model captures the characteristics of rainfall events over the entire Guinea Coast. After evaluating CMIP6 GCMs, Ajibola *et al.* (2020) found that these models can reproduce wet and dry conditions over WA. However, the GCMs typically have issues in reproducing the main WAM features, probably due to the coarse grid spacing that is usually used (Cook and Vizy 2006; Hourdin *et al.* 2010; Sylla *et al.* 2010, 2013; Xue *et al.* 2010; Chagnaud *et al.* 2020). For example, Cook and Vizy (2006), after evaluating several GCMs, found that most models fail to represent the precipitation over WA properly. Xue *et al.* (2010), after evaluating how well several GCMs simulate the characteristics of the WAM, found that most models struggle to reproduce the intensities of the AEJ and the tropical easterly jet (TEJ). Arguing that using regional climate models (RCMs) with a higher resolution than GCMs may be a solution to the resolution problem, some studies have employed and evaluated RCMs over WA (Afiesimama *et al.* 2006; Pal *et al.* 2007; Abiodun *et al.* 2010; Sylla *et al.* 2010, 2012; Diallo *et al.* 2012; Klutse *et al.* 2016; Odoulami *et al.* 2019; Tamoffo *et al.* 2022). Sylla *et al.* (2010) found that RegCM3 realistically simulates the precipitation over the region, but other studies noted some uncertainties in the simulation (Pal *et al.* 2007; Browne and Sylla 2012; Odoulami *et al.* 2019). Pal *et al.* (2007) found that RegCM3 produces excess precipitation over WA. Odoulami *et al.* (2019) found that the models generally overestimate the magnitudes of the rainfall indices over the Guinea Coast. Browne and Sylla (2012) attributed the precipitation biases in RCMs to boundary condition problems. Hence, the attempt to address the low-resolution problem of GCMs and the boundary conditions problem of RCMs has prompted several studies to utilize stretched-grid GCMs (SG-GCMs) (e.g., Fox-Rabinovitz *et al.* 2006, 2008; Abiodun *et al.* 2011; Smith *et al.* 2013; Martini *et al.* 2015; Harris *et al.* 2016).

The Model for Prediction Across Scales (MPAS) is a good example of SG-GCM. MPAS is also known for its quasi-equal distance between grids, which eliminates the problem of ‘pole singularity’ at the poles where the grids converge. This

singularity usually causes numerical instability and computational challenges (Kramer *et al.* 2020). In addition, the stretched-grid capability of MPAS allows for two-way interaction between the regional scale features over the high-resolution area and the large-scale motion outside the area (Heinzeller *et al.* 2016). However, MPAS is becoming more prominent for studying regional atmospheric features. It has been used to simulate and study tropical cyclones (Davis and Birner 2016; Michaelis *et al.* 2019; Lui *et al.* 2021; Donkin and Abiodun 2023), Intertropical Convergence Zones, the Madden–Julian Oscillation, and the West African Monsoon (Landu *et al.* 2014; Heinzeller *et al.* 2016; Pilon *et al.* 2016). All these studies conclude that MPAS gives realistic simulations of these atmospheric features. In addition, Lui *et al.* (2021) found that MPAS performs better than the Weather Research and Forecasting (WRF) model in reproducing the western North Pacific tropical cyclone model. Despite the potential of MPAS for regional scale studies, only Heinzeller *et al.* (2016) has evaluated the performance of the model in West Africa, and the evaluation only cover one season. The present study intends to build on Heinzeller *et al.* (2016) by testing the model capability over a longer period.

Hence, the present study aims to investigate the performance of MPAS in simulating the WAM system, its associated features, and the precipitation over WA compared to four AMIP (Atmospheric Models Intercomparison Project) models. The article is structured as follows: Section 2 describes the paper’s methodology, section 3 presents and discusses the results, and section 4 provides the conclusions.

## 2. Materials and methods

### 2.1 Model description and experiments

The Model for Prediction Across Scales-Atmosphere (MPAS-A) is used in this study. It is a non-hydrostatic atmosphere model (Klemp and Skamarock 2021) that is one of the components of the Earth-system models generally denoted as MPAS. MPAS uses centroidal Voronoi tessellations for its horizontal meshes (Thuburn *et al.* 2009; Ju *et al.* 2011). A 60-km uniform resolution mesh with 1,63,842 cells is used for the run. We utilized the mesoscale ‘reference physics’ suite with 55 vertical and four soil levels. For the terrain, we applied the

Land-Surface Model (*Noah*-LSM) (Chen *et al.* 1996).

The associated parameterization schemes are summarized in table 3. This configuration is used in the work of Heinzeller *et al.* (2016). The radiation (long-wave, short-wave) scheme uses a constant value for carbon dioxide, which represents the atmospheric CO<sub>2</sub> concentration around 2004. The static input data are from the Moderate Resolution Imaging Spectroradiometer (MODIS) 20-class land cover product, which depends on the global land cover climatology collected from 2001 to 2010 at a resolution of 500 m (Broxton *et al.* 2014) and the Global Multi-Resolution Terrain Elevation Data (GMTED2010) (Danielson and Gesch 2011) topography. The albedo and vegetation indices are updated using the monthly climatology of MODIS satellite images.

The experiment is a continuous simulation that was initialized with the NCEP, CFSR (Nation Center for Environmental Prediction, Climate Forecast System Reanalysis) data available from <https://rda.ucar.edu/datasets/ds093.1/>. The model was set to periodically update using 6 hours of CFSR Sea Surface Temperature (SST) and sea-ice data for realistic results. The simulation ran from December 1, 1980, to January 31, 2011, with data analysed between January 1981 and December 2010. December 1, 1980 is considered a spin-up.

To quantitatively assess MPAS, we evaluate the spatial pattern, the annual cycle and the simulation bias by using quantitative measures such as the mean bias (MB), root mean square error (RMSE), and spatial correlation coefficient ( $r$ ) with respect to the Climate Hazards Group InfraRed Precipitation with Stations (CHIRPS) rainfall. These quantitative measures allow to measure model systematic errors and performance as they provide information at both regional and grid point levels (Browne and Sylla 2012). The capability of MPAS in simulating the WAM features will be investigated through the monsoon flow, AEJ, TEJ, and upward motion. We also investigate how MPAS performs in simulating the origin of the jets, which include the zonal wind, temperature gradient, and thermal wind with respect to the European Centre for Medium-Range Weather Forecasts version 5 (ERA5). MPAS does not provide output for thermal winds. Therefore, the following formulas have been used to determine the thermal winds between the surface 925 and 700 hPa.

$$Ut = -(R/f)(\partial T_m/\partial y)(\ln P_{925}/P_{700}) \quad (1)$$

$$Vt = (R/f)(\partial T_m/\partial x)(\ln P_{925}/P_{700}) \quad (2)$$

where  $f$  is the Coriolis force parameter ( $7.29 \times 10^{-5} \text{ s}^{-1}$ );  $\rho$  is the air density ( $1.2 \text{ kg m}^{-3}$ ),  $g$  is the gravity ( $9.8 \text{ m s}^{-2}$ ),  $R$  is the gas constant ( $8.3144598 \text{ J mol}^{-1} \text{ K}^{-1}$ ),  $P_{925}$  and  $P_{700}$  are respectively pressure at 925 and 700 hPa, the term  $(\partial T_m/\partial y)$  is the mean temperature ( $T_m$ ) gradient in  $y$  direction.

## 2.2 Study area

The study was conducted in WA (figure 1). Due to climatic differences, the region is subdivided into three zones: the Guinea Coast zone (4–8°N), the Savanna zone (8–11°N), and the Sahel zone (11–16°N). Previous studies have considered these areas (Sylla *et al.* 2010; Abiodun *et al.* 2011; Gbode *et al.* 2019; Ajibola *et al.* 2020). The Guinea Coast zone is humid, with annual rainfall ranging from 1575 to 2533 mm (Oguntunde *et al.* 2011; Gbode *et al.* 2019), and the Savanna zone is a semi-arid area, with average annual rainfall in the range of about 897–1535 mm (Nicholson 2009). The northward displacement of the rainfall belt thus initiates the recognized ‘little dry season’ and ‘peak of rainy season’ between July and August along the Guinea Coast and Savanna, respectively (Gbode *et al.* 2019). The Sahel zone is characterized by a single peak season from July to September, with a maximum in August that coincides with the

northernmost location of the Intertropical Discontinuity (ITD) from 21–22°N (e.g., Nicholson 2013). This area is arid compared to the two zones mentioned above, and the Sahel zone has an average annual rainfall between 434 and 969 mm (Oguntunde *et al.* 2011; Gbode *et al.* 2019). We focus on the June–July–August (JJA) season because it provides the most significant precipitation amounts over WA, especially over the Sahel zone (Nicholson 2013).

## 2.3 Applied data

For this study, we evaluate MPAS performance using different observations and reanalyses datasets. The observed data are either gauge-based or satellite-derived (table 1), and they include the Climate Hazards Group InfraRed Precipitation with Station (CHIRPS) and the Climate Research Units (CRU) data. Variables such as zonal and meridional wind components ( $u$ ,  $v$ ), the vertical wind velocity, and the geopotential height ( $z$ ) were obtained from reanalyses (table 1), including the European Centre for Medium-Range Weather Forecasts (ECMWF) reanalysis v5 (ERA5) and the CFSR. To put MPAS in the context of GCMs, four AMIP (Atmospheric Model Intercomparison Project, table 2) models are also used for comparison (Niang *et al.* 2017). All the datasets were interpolated to a resolution of  $0.5^\circ \times 0.5^\circ$  using the first-order conservative remapping method (Jones 1999).

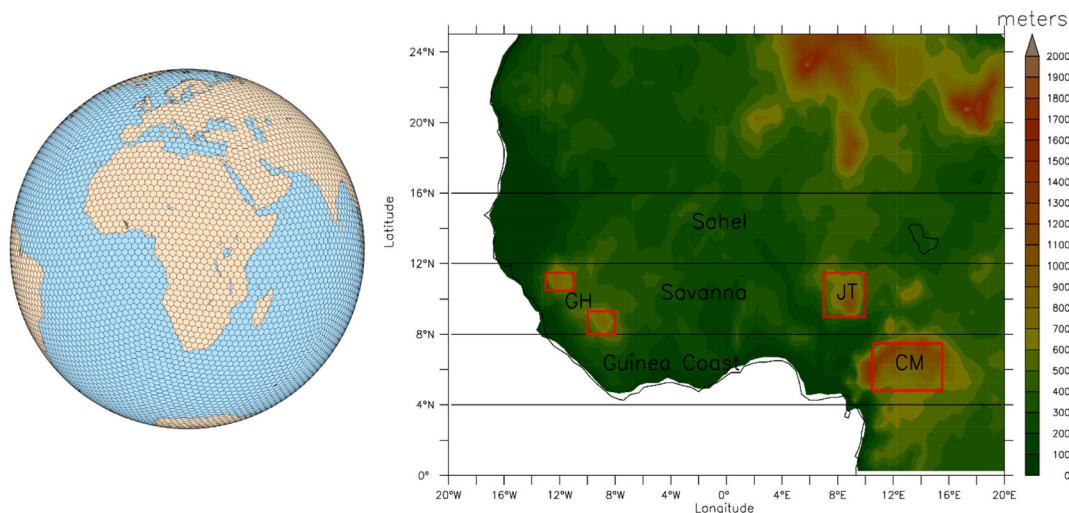


Figure 1. The quasi-uniform mesh with a resolution of 60 km used for the MPAS simulation (left) and the topography of the investigated area for three sub-regions: the Sahel, Savanna, and Guinea Coast zones (right). Red boxes are showing the Guinea Highland (GH), Jos Plateau (JP), and Cameroon Mountains (CM).



Table 1. *Observed and reanalysis data applied in the present study (from 1981 to 2010).*

Dataset	Name	Horizontal resolution	Reference
CHIRPS	Climate Hazards Infrared Precipitation with Stations	0.25°	Funk <i>et al.</i> (2015)
CRU	Climate Research Unit	0.5°	Harris <i>et al.</i> (2020)
ERA5	European Centre for Medium-Range Weather Forecast (ECMWF)	0.25°	Hersbach <i>et al.</i> (2020)
CFSR	Climate Forecast System Reanalysis	0.5°	Saha <i>et al.</i> (2014)

Table 2. *AMIP data used in this study (from 1979 to 2008).*

Models	Institutes	Lat. × Lon.
BBC-CSM1-1-M	Beijing Climate Center, China Meteorological Administration	1.1° × 1.25°
HadGEM2-A	Met Office Hadley Centre	1.25° × 1.875°
IPSL-CM5A-LR	Institut Pierre Simon Laplace	1.875° × 3.75°
NorESM1-M	Norwegian Climate Centre	1.9° × 2.5°

Table 3. *Parametrization schemes used by the simulations.*

Parametrization	Scheme
Convection	New Tiedtke
Microphysics	WSM6
Land surface	Noah-LSM
Boundary layer	YSU
Surface layer	Monin–Obukhov
Radiation, LW	RRTMG
Radiation, SW	RRTMG
Cloud fraction for radiation	Xu–Randall
Gravity wave drag by orography	YSU

### 3. Results

#### 3.1 Rainfall patterns

In this section, we discuss the ability of MPAS to simulate the seasonal rainfall and spatial pattern of the WAM over WA. We apply two observational datasets (CHIRPS and CRU) to evaluate MPAS. In addition, two reanalyses (ERA5 and CFSR) are used as the intermediate data between the observed data and model output. CHIRPS is used as a reference because of its high horizontal grid resolution (0.25°). The resolution of CHIRPS reduces error during interpolation (Tamoffo *et al.* 2022).

##### 3.1.1 Annual cycle of rainfall and zonal winds

All the observational datasets (figure 2) show that WA rainfall exhibits three main phases (the

onset, the peak, and the retreat), consistent with previous studies (Sylla *et al.* 2009; Abiodun *et al.* 2011). MPAS realistically reproduces three phases (figure 2i). For instance, as in the observed datasets, the simulated onset is from March to June in MPAS, and it is characterized by the northward extension of the rain belt from the coast (6°N). The simulated peak is characterized by a northward (10°N to 14°N) jump of the rain belt and the end of the rainfall between the equator and 6°N, which is underestimated and does not completely disappear in comparison with observed data. The peak in MPAS occurs between June and September, which is consistent with the observations. In addition, MPAS shows good performance in simulating the bimodality of rainfall over Guinea (figure 2j) and the unimodality of rainfall over the Savanna (figure 2k) and Sahel zones (figure 2l), as depicted in the observations. However, a stronger dip is noted in the MPAS simulated annual cycle over the Guinea Coast (figure 2j) and Savanna (figure 2k), but it never reaches zero. The biases range from −1 to −5 mm/day, exceeding the observed data differences of −1 mm/day. MPAS performs better than most AMIP models in simulating the annual cycle of monsoon rainfall (MPAS:  $r = 0.88$ , RMSE = 1.71 mm/day; BCC-CSM1-1-M:  $r = 0.87$ , RMSE = 1.95 mm/day; IPSL-CM5A:  $r = 0.85$ , RMSE = 2 mm/day; NorESM1-M:  $r = 0.87$ , RMSE = 1.97 mm/day, relative to CHIRPS). The dry bias of the monsoon rainfall is

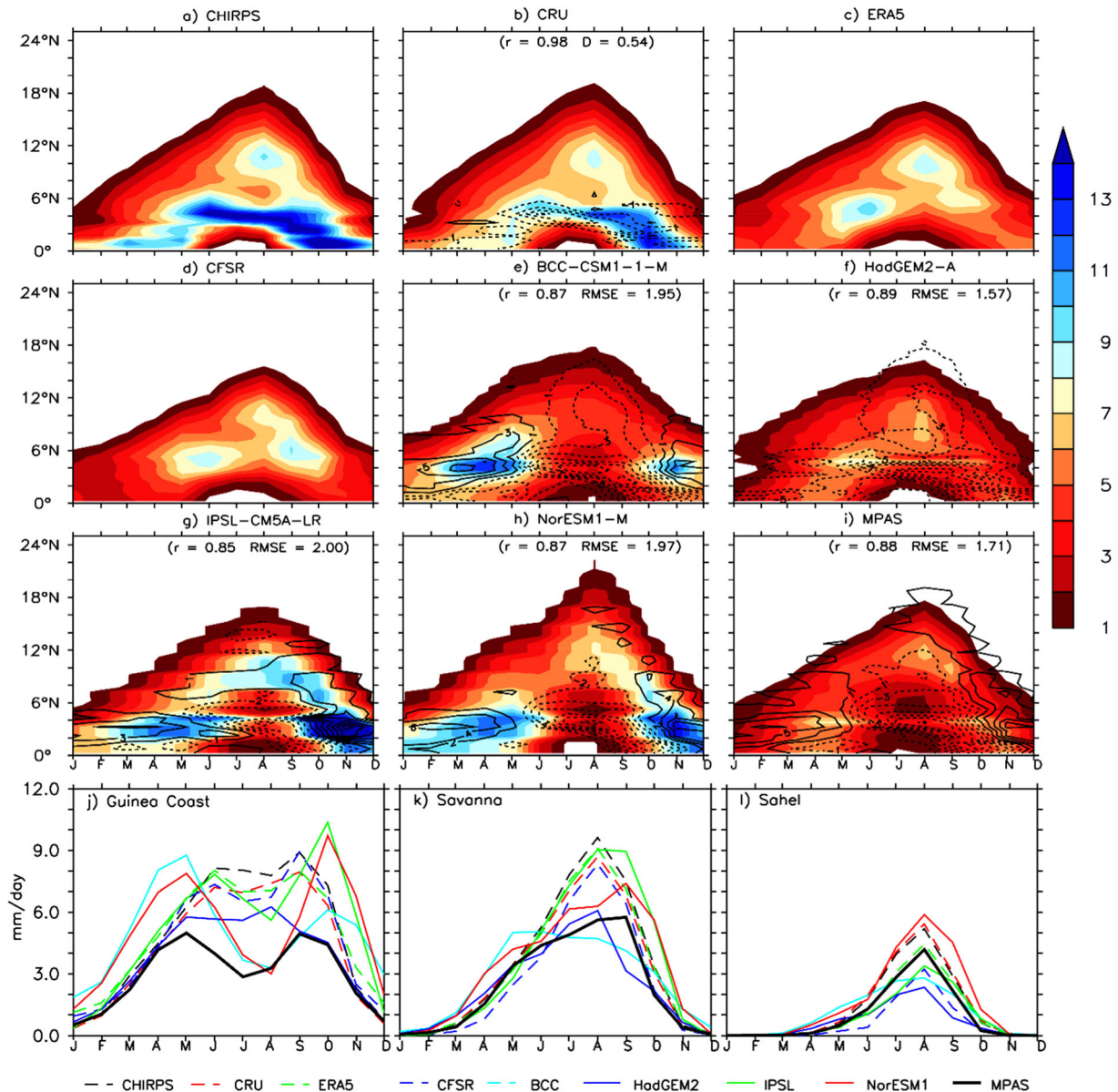


Figure 2. Hovmoller diagrams of daily precipitation (mm/day) averaged from 10°W–10°E for (a) CHIRPS, (b) CRU, (c) ERA5, (d) CFSR, (e) BCC-CSM1-1-M, (f) HadGEM2-A, (g) IPSL-CM5A-LR, (h) NorESM1-M, and (i) MPAS. The bias between the datasets and CHIRPS is represented using contours. The values in brackets represent the spatial correlation coefficient ( $r$ ) and the root mean square error (RMSE) relative to CHIRPS. The monthly mean variation of area-averaged rainfall (mm/day) is represented at the bottom: (j) Guinea Coast, (k) Savanna zone, and (l) Sahel zone. The period 1981–2010 is used for the reanalyses, the observations, and MPAS, and the period 1978–2008 is used for AMIP.

a common problem found in many GCMs and RCMs (Abiodun *et al.* 2010; Sylla *et al.* 2010; Abatan 2011; Ajibola *et al.* 2020). For instance, Sylla *et al.* (2010) found that RegCM3 underestimates the rain rate during the onset period. Abiodun *et al.* (2010) found that finite volume dynamics (CFV) GCMs fail to capture the maximum monsoon peak. Ajibola *et al.* (2020) found that most CMIP6 models underestimate the rainfall over WA. The dry biases in GCMs have

been attributed to the coarse grid spacing and boundary layer of the models (Diallo *et al.* 2012; Sylla *et al.* 2013).

The zonal winds are usually strong between 600 and 700 hPa (Cook 1999) and have been analysed in the work of Raj *et al.* (2019). MPAS (figure 3g) reasonably simulates the pattern of the annual cycle of zonal wind, which characterize the monsoon flow at 700 hPa. For instance, the peak in August and the southward retreat are reasonably

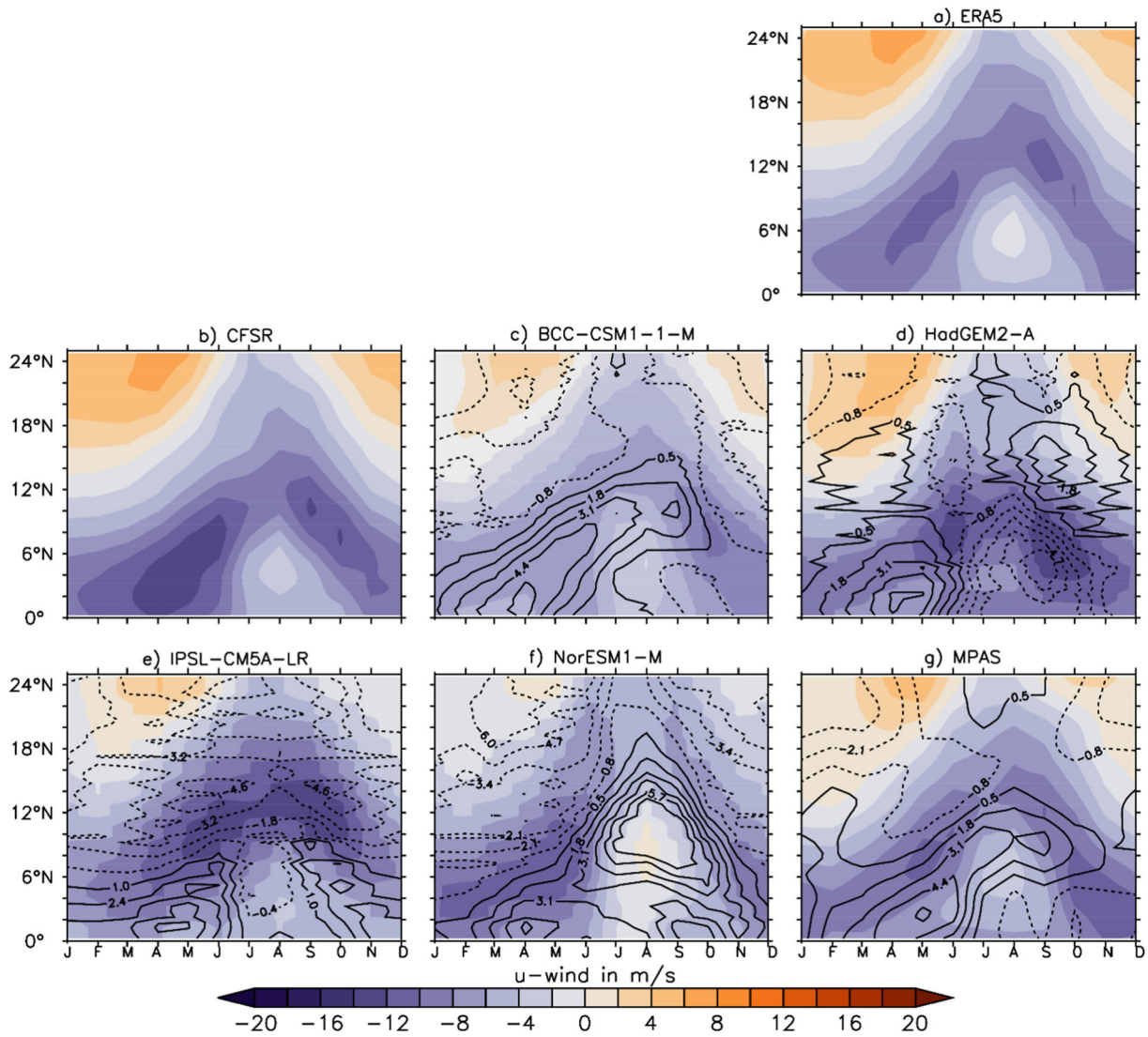


Figure 3. Time-latitude diagrams of monthly mean zonal wind (m/s; shaded) at 700 hPa, averaged from 10°W–10°E for (a) ERA5, (b) CFSR, (c) BCC-CSM1-1-M, (d) HadGEM2-A, (e) ISPL-CM5A-LR, (f) NorESM1-M, and (g) MPAS. The contours indicate the bias between ERA5 and the other models. The period 1981–2010 is used for the reanalyses, the observations, and the MPAS, and the period 1978–2008 is used for AMIP.

simulated. However, MPAS reproduces north-easterly winds from January to March and from October to December over the Sahel zone with lower magnitudes; the bias (figure 3g, contours) is up to 2 m/s relative to ERA5. MPAS also underestimates the strength of the monsoon flow (–8 m/s) during the peak period of August over the Sahel and Savanna zones compared to ERA5 (–12 m/s).

Additionally, MPAS and most AMIP models overestimate the magnitude of the zonal wind over the Guinea Coast (around 5°N) and in one part of Savanna (around 11°N) with regards to ERA5, underestimation of the north-easterly wind (between 24° and 18°N) is also noted in AMIP models.

The underestimation of the monsoon flow and the north-easterly wind may contribute to MPAS’s shortcomings in representing the peak of the monsoon rainfall over WA. These results are in agreement with previous studies (Raj *et al.* 2019; Tamoffo *et al.* 2022). For instance, Raj *et al.* (2019) found that the Earth System Model (ESM2M) shows a northward shift of the zonal wind during the peak intensity over WA.

### 3.1.2 Seasonal pattern of WAM rainfall

Figure 4(a)–(i) shows the JJA precipitation climatology from CHIRPS, CRU, ERA5, CFSR, the AMIP models, and MPAS. MPAS reasonably



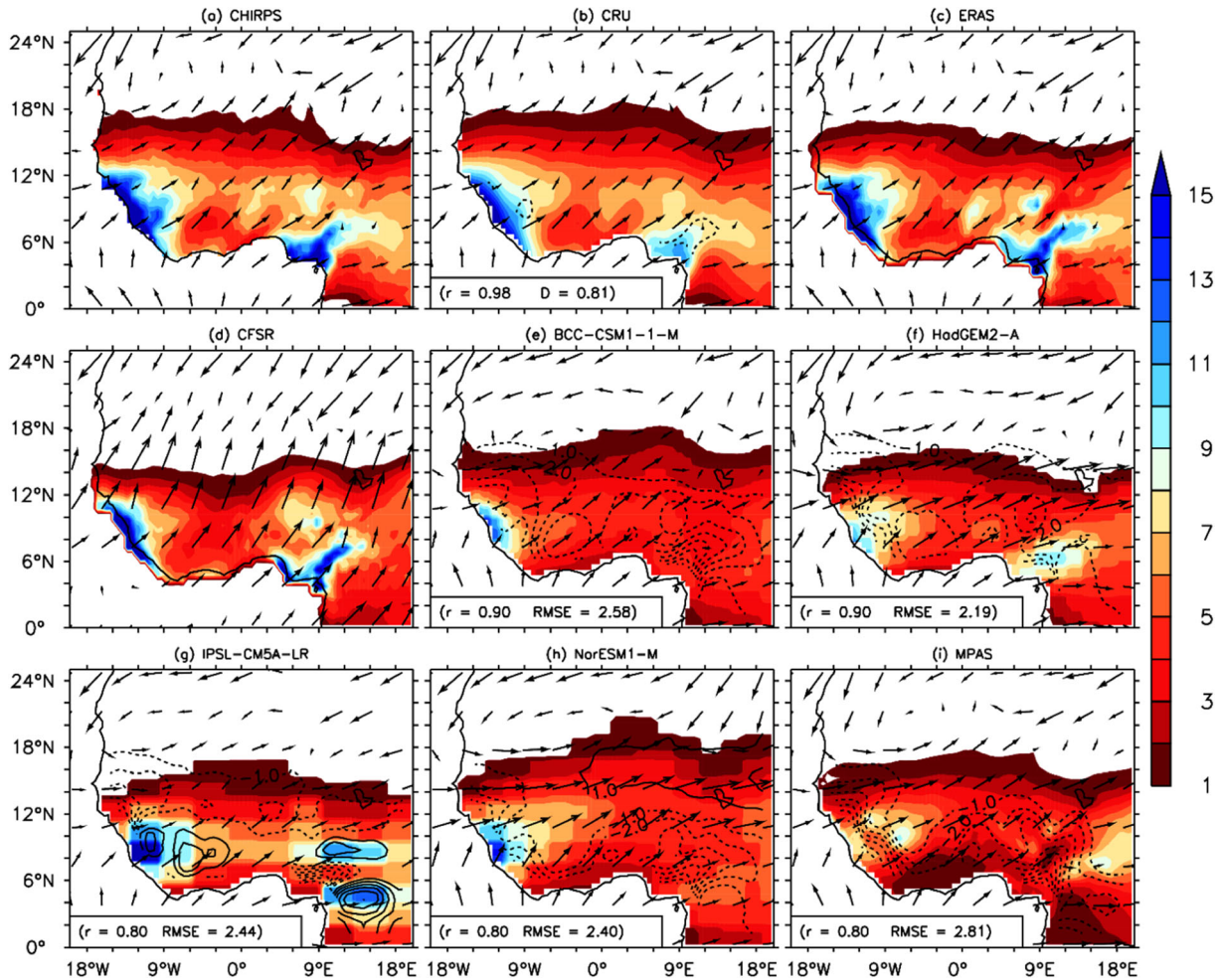


Figure 4. Averaged JJA precipitation (mm/day) for (a) CHIRPS, (b) CRU, (c) ERA5, (d) CFSR, (e) BCC-CSM1-1-M, (f) HadGEM2-A, (g) IPSL-CM5A-LR, (h) NorESM1-M, and (i) MPAS. The bias between the datasets and CHIRPS is represented by contours. The vectors showing the monsoon flow represent the U (u-winds) and V (v-winds) components of wind in August at 850 hPa. Wind data from ERA5 overlay the CHIRPS and CRU rainfall. The values in the boxes represent the spatial correlation coefficient ( $r$ ) and the root mean square error (RMSE) relative to CHIRPS. The period 1981–2010 is used for the reanalyses, observations, and MPAS, and the period 1978–2008 is used for AMIP.

simulates the regional migration of rainfall modulated by the rainband movement (see vectors of meridional and zonal components of winds at 850 hPa). The position of the rainband is also reasonably simulated during the other seasons (not shown). In addition, MPAS reproduces the rainfall amounts around 12–16°N and 9–20°E that are given by the observed data. However, MPAS underestimates the peak height (5 mm/day) of the orographic rainfall (Guinea Highlands, Mount Cameroon, Jos Plateau) compared to the observed (11 mm/day) data and the reanalysis (10 mm/day). This underestimation of rainfall over the mountains is a common issue with global models, especially if they are used with coarser resolution (case of MPAS). The bias in MPAS ranges from  $-1$  to  $-3$  mm/day, which is out of the range of the uncertainties between the observed

data. When it comes to simulating the spatial pattern of the seasonal rainfall, MPAS and AMPI models show almost the same pattern (MPAS:  $r = 0.80$ , RMSE = 2.81 mm/day; BCC-CSM1-1-M:  $r = 0.90$ , RMSE = 2.19 mm/day; IPSL-CM5A:  $r = 0.80$ , RMSE = 2.44 mm/day; NorESM1-M:  $r = 0.80$ , RMSE = 2.40 mm/day, relative to CHIRPS). The issue with simulating the spatial variability of the WAM rainfall is a common problem within GCMs, which struggle to reproduce mesoscale and local processes due to their coarse grid resolutions, in the case of MPAS resolution used in this study. Our results align with those of previous studies (Vizy and Cook 2002; Sylla *et al.* 2013; Klutse *et al.* 2021). For instance, Sylla *et al.* (2010) found that CMIP models miss the maxima over Mount Cameroon due to their low spatial resolution. Klutse *et al.*



(2021) found that GCMs have difficulty simulating mountainous rainfall over West Africa.

### 3.2 West African Monsoon features

In this subsection, we evaluate how well MPAS captures the climatology of the wind system over WA. We investigate why MPAS has shortcomings when it comes to reproducing rainfall climatology over the study zones. Therefore, we address the dynamics of upper and mid-tropospheric easterly jets (TEJ, AEJ) and the low levels of the monsoon flow (Cook 1999; Nicholson and Grist 2003; Akinsanola *et al.* 2017), using ERA5 as a reference.

The core of the AEJ (>10 m/s) is located at around 15°N and 600 hPa in the reanalyses and some AMIP models (IPSL-CM5A-LR, NorESM1-M) (figure 5). The AEJ is of crucial importance because the model’s wetness and dryness over the Sahel seems to be driven in most of the case by poleward and equatorward displacement of AEJ and the jet magnitude (Abiodun *et al.* 2010;

Tamoffo *et al.* 2022). The lack of MPAS output at 600 hPa pressure level weakens the analysis of the AEJ in the model. MPAS (figure 5(j)) shows the location of the TEJ at the same altitude (~200 hPa) as that of ERA5 but underestimates the speed (-2 m/s), while the AMIP models show southward shifting of the TEJ core and overestimate the speed (1–4 m/s). Underestimating the strength and mislocating the location of TEJ in the models compared to reanalyses could contribute to the rainfall biases as this jet is of great importance in the West African rainfall-producing system (Nicholson 2009; Sylla *et al.* 2009). MPAS and the AMIP models (BCC-CSM1-1-M, HadGEM2-A) overestimate (2–5 m/s) the low-level (850 hPa) monsoon flow at around 4° to 12°N, located between 4 and 11°N in ERA5. The MCSs are favoured by a weaker TEJ during the summer. The MCSs (squall lines, mesoscale convective complexes) cross the region (Janicot 1997) during summer; therefore, underestimating them and misrepresenting the TEJ location in MPAS may contribute to the shortcomings in simulating the rainfall

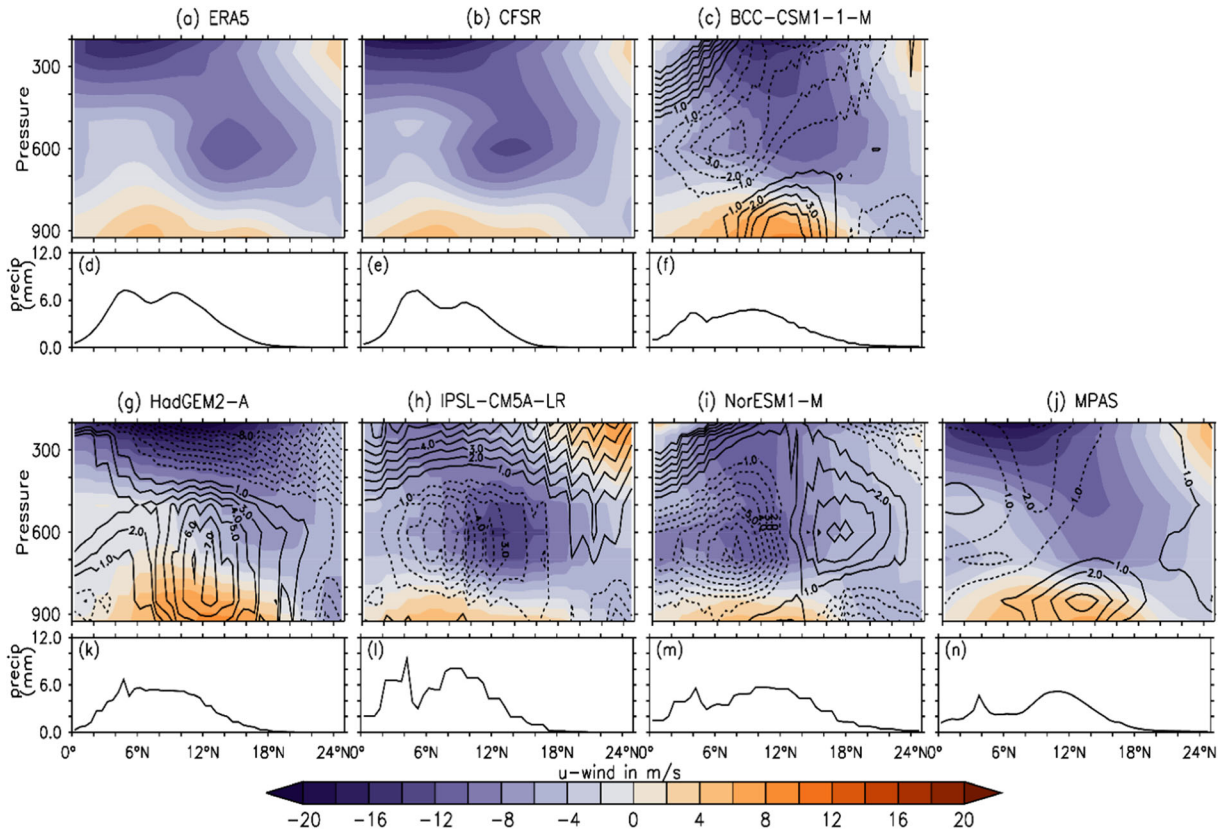


Figure 5. Latitude-height cross-section of the zonal wind (m/s, shaded) in August averaged from 10°W–10°E. The datasets are from (a) ERA5, (b) CFSR, (c) BCC-CSM1-1-M, (g) HadGEM2-A, (h) ISPL-CM5A-LR, (i) NorESM1-M, and (j) MPAS, figures (d), (e), (f), (k), (l), (m) and (n) represent the seasonal (JJA) precipitation (mm/day) respectively. The contours represent the bias between ERA5 and each dataset, and the pressure is given in hPa. The period 1981–2010 is used for the reanalyses, observation, and MPAS, and the period 1978–2008 is used for AMIP.

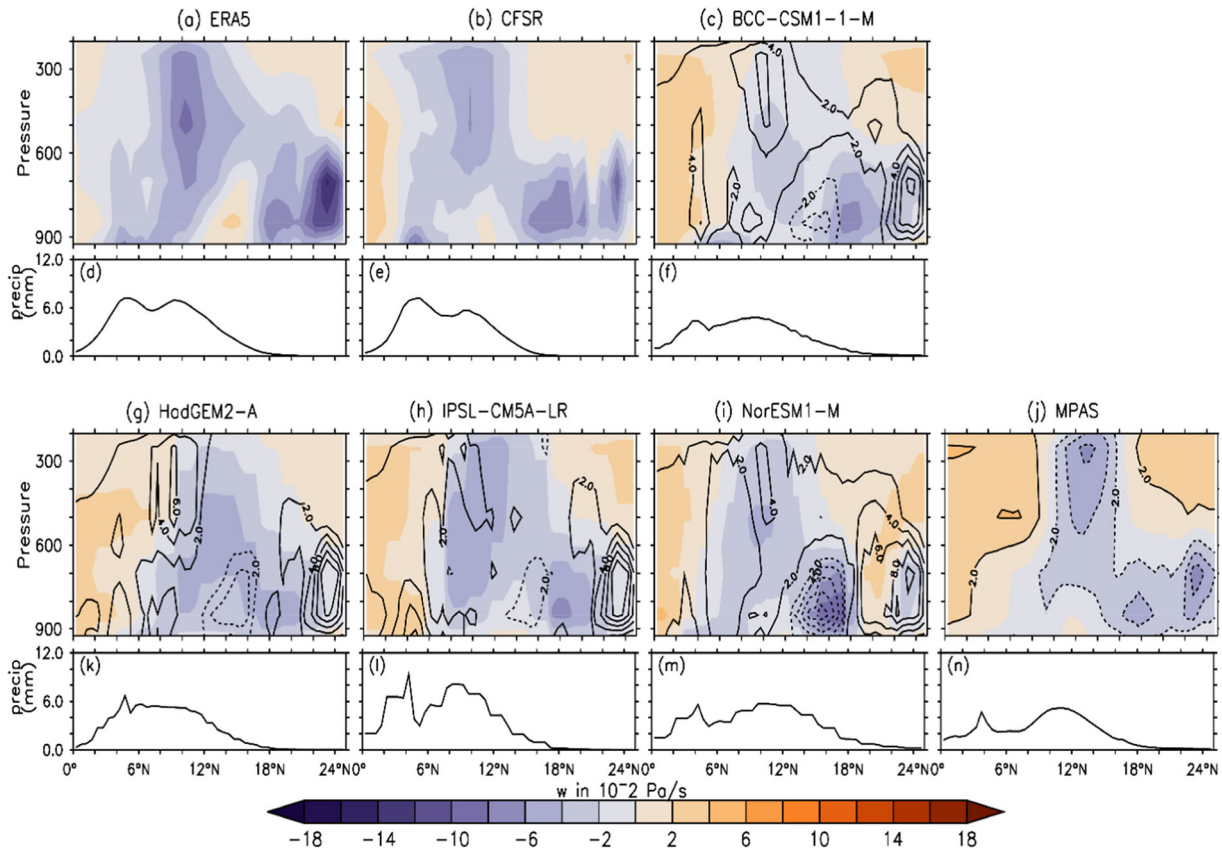


Figure 6. The latitude height of vertical velocity ( $w$  in Pa/s, shaded) in August averaged from  $10^{\circ}\text{W}$ – $10^{\circ}\text{E}$ . The datasets are from (a) ERA5, (b) CFSR, (c) BCC-CSM1-1-M, (g) HadGEM2-A, (h) IPSL-CM5A-LR, (i) NorESM1-M, and (j) MPAS, figures (d), (e), (f), (k), (l), (m) and (n) represent the seasonal (JJA) precipitation (mm/day) respectively. The contours represent the bias between ERA5 and the other models. As the units are Pa/s, negative values of omega represent upward motion. The period 1981–2010 is used for the reanalyses, observations, and MPAS, and the period 1978–2008 is used for AMIP.

(figures 2(j)–(l) and 5(n)) during the peak period over the Savanna and Sahel regions.

Figure 6 shows the vertical cross-section of vertical velocity (Pa/s) as a function of latitude for August. Generally, all the datasets capture two ascent regions, as shown in ERA5. The ascent corresponds to the response of convection to local atmospheric circulation (Tamoffo *et al.* 2022). MPAS (figure 6j) shows the first ascent, which is south of  $24^{\circ}\text{N}$  (between 900 and 700 hPa), as in ERA5 (figure 6a), and corresponds to the Intertropical Discontinuity (ITD) caused by dry convection in the Saharan heat low (Sylla *et al.* 2010; Abiodun *et al.* 2011). Next, MPAS locates the second ascent between the surface and 300 hPa as in ERA5 and other models; it results from deep convection over the Sahel zone ( $12^{\circ}\text{N}$ ). However, MPAS underestimates (by up to 2 Pa/s) the vertical velocities of the two ascent zones compared to ERA5. The underestimation of the upward motion might be linked to the coarser resolution of MPAS compared to 25 km ERA5. All the AMIP models fail to locate the ascent zones as depicted in ERA5; these issues might

likely come from the coarser resolution of these atmospheric models. Overall, the dry biases in MPAS may be related to the weak simulation of the convective activities due to the coarser resolution. Our results are in line with the findings of Tamoffo *et al.* (2022), who showed the issues of some RCMs to simulate the vertical motion over West Africa.

### 3.3 Thermal activities during summer

In this subsection, we look at how MPAS simulates the thermal activities in summer to determine if the issues (rainfall biases, weak jets, strong low-level wind) detected in the previous analysis occur because MPAS struggles to represent some of the processes that contribute to the dynamics of the WAM. For instance, we look at how MPAS simulates the zonal wind over WA, the temperature gradient, and the thermal wind.

Figure 7 shows the zonal wind at 700 hPa for August (1981–2010) from (a) ERA5 and (b) MPAS. MPAS reasonably ( $r = 0.98$ ) simulates

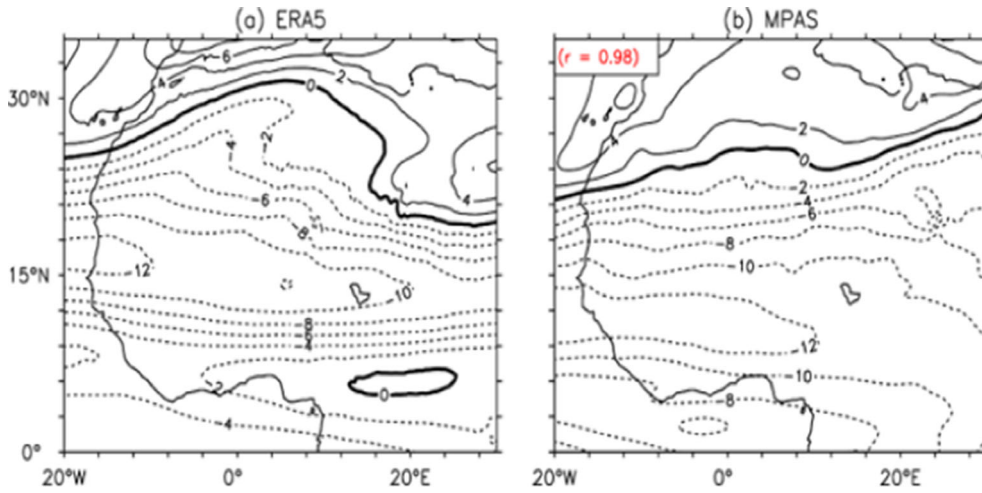


Figure 7. Zonal wind field (m/s) at 700 hPa in August for (a) ERA5 and (b) MPAS.

the spatial pattern of the zonal wind over WA, which is in agreement with ERA5. The core of the jet is located at around 15°N in ERA5. It is very difficult to discuss the core of AEJ in MPAS due to the inexistence of 600 hPa level in the model. MPAS places the boundary separating the westerly and easterly flows of zonal wind farther north (between 20°E and 30°E) than ERA5. In addition, MPAS did not place the jets in the north at around 26°N (Egyptian desert) as ERA5 did. A weaker jet might transport less moisture, resulting in less rainfall in the model (Tamoffo *et al.* 2022), which might cause dry biases in MPAS over the Sahel zone. Tamoffo *et al.* (2022) mentioned that dry biases over the Sahel zone are affected by the poleward or equatorward movement of the AEJ and the jet strength. Overall, the underestimation of the jet strength in MPAS may impact the number of mesoscale convective systems (MCSs) and then reduce the amount of rainfall over the Sahel zone, where the MCSs contribute enormously to the development of the rainy season (Nicholson and Webster 2007; Tamoffo *et al.* 2022). The results are consistent with those of Tamoffo *et al.* (2022), who found that the dry bias in RCMs is associated with weaker AEJ activities in the models.

Figure 8 depicts the meridional temperature gradient at 850 hPa, averaged from 10°W to 10°E. MPAS reasonably simulate ( $r = 0.83$ ) the spatial pattern of the meridional temperature gradient in agreement with ERA5. MPAS shows the minimum (2 K/[1000 km]) gradient in January and December, as in ERA5, but MPAS seems colder than ERA5; for instance, it underestimates the

maximum gradient (8 K/[1000 km]) in June compared to ERA5 (10 K/[1000 km]). This result is in line with the work of Nicholson and Grist (2003), who found the same result in their analysis of the meridional temperature gradient in the NCEP–NCAR reanalysis. We also explore the meridional temperature gradient during the summer months. Figure 9 shows the meridional gradient of temperature from June to August at 850 hPa. MPAS reasonably simulates the spatial pattern of the monthly temperature gradient, but it loses the location of the gradient farther north, which is shown by ERA5.

In contrast to ERA5, MPAS simulates the temperature gradient at almost the same location in the north for all months. The misplacement of the meridional temperature gradient in MPAS can influence the atmospheric circulation in the Sahelian zone because this gradient is responsible for the formation of the jet (Nicholson and Grist 2003) and is among the factors that contribute to triggering the moisture advection from the Atlantic Ocean to the continent (Nicholson 2009). The origin of the AEJ in the Northern Hemisphere is essentially the temperature gradient caused by the difference between the Sahara and the humid Guinea Coast to the south (Thorncroft and Blackburn 1999). Thus, a weaker temperature gradient may lead to a weaker jet, which may transport less moisture and contribute to the dry biases in MPAS.

Figure 10 shows the thermal wind between two pressure levels, 500 and 925 hPa, and 700 and 925 hPa. For the thermal wind between 500 and 925 hPa, MPAS simulates the magnitude given by



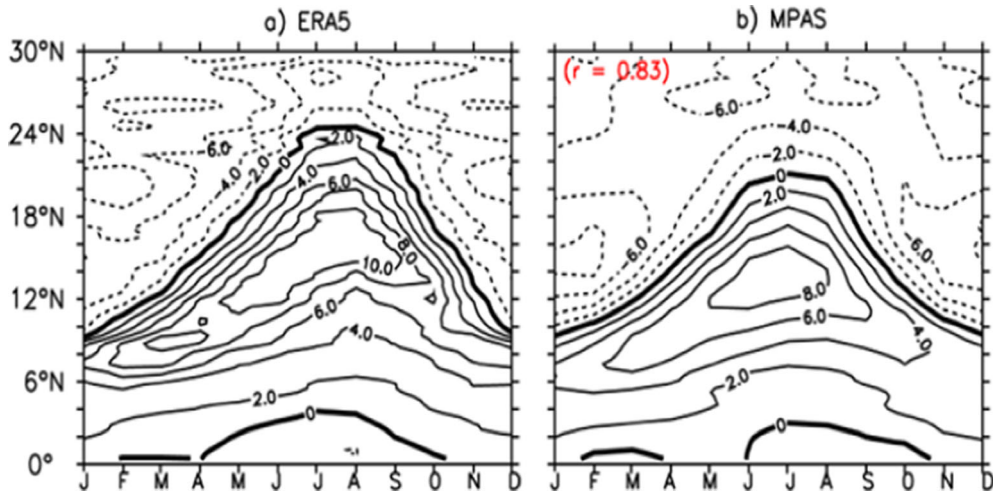


Figure 8. The time latitude of the meridional temperature gradient (K/[1000 km]) at 850 hPa, averaged from 10°W–10°E, for (a) ERA5 and (b) MPAS.

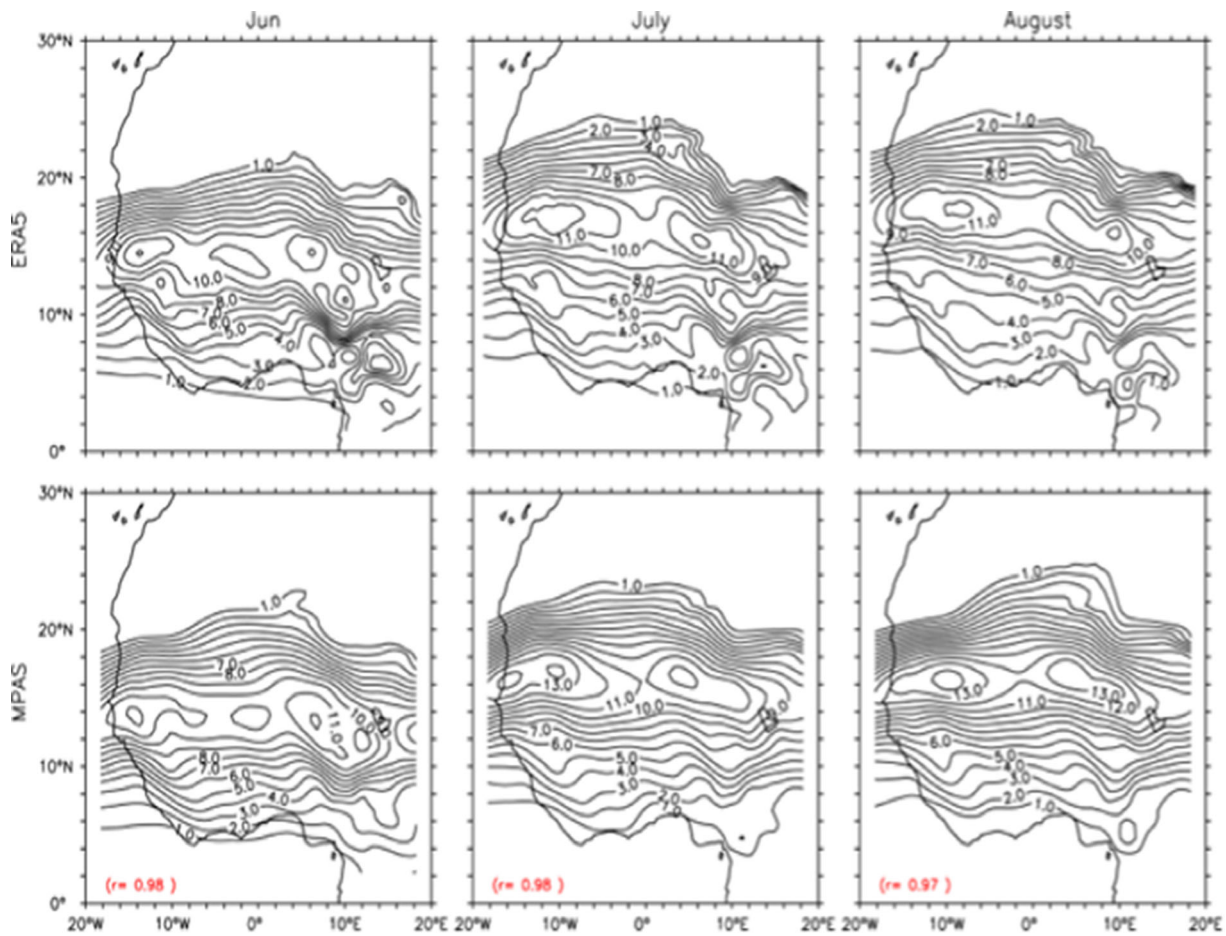


Figure 9. Month-to-month (June, July, August) spatial distribution of the temperature gradient (K/[1000 km]) for ERA5 (first row) and MPAS (second row).

ERA5 (>25 m/s), but the thermal wind does not extend as far eastward and northward as it does in ERA5. However, the thermal wind simulated by MPAS between 700 and 925 hPa is the opposite of

the thermal wind between 500 and 925 hPa; simulating a small area of the thermal wind between these levels may influence the formation of the wind shear and hence the easterly jets, and it may

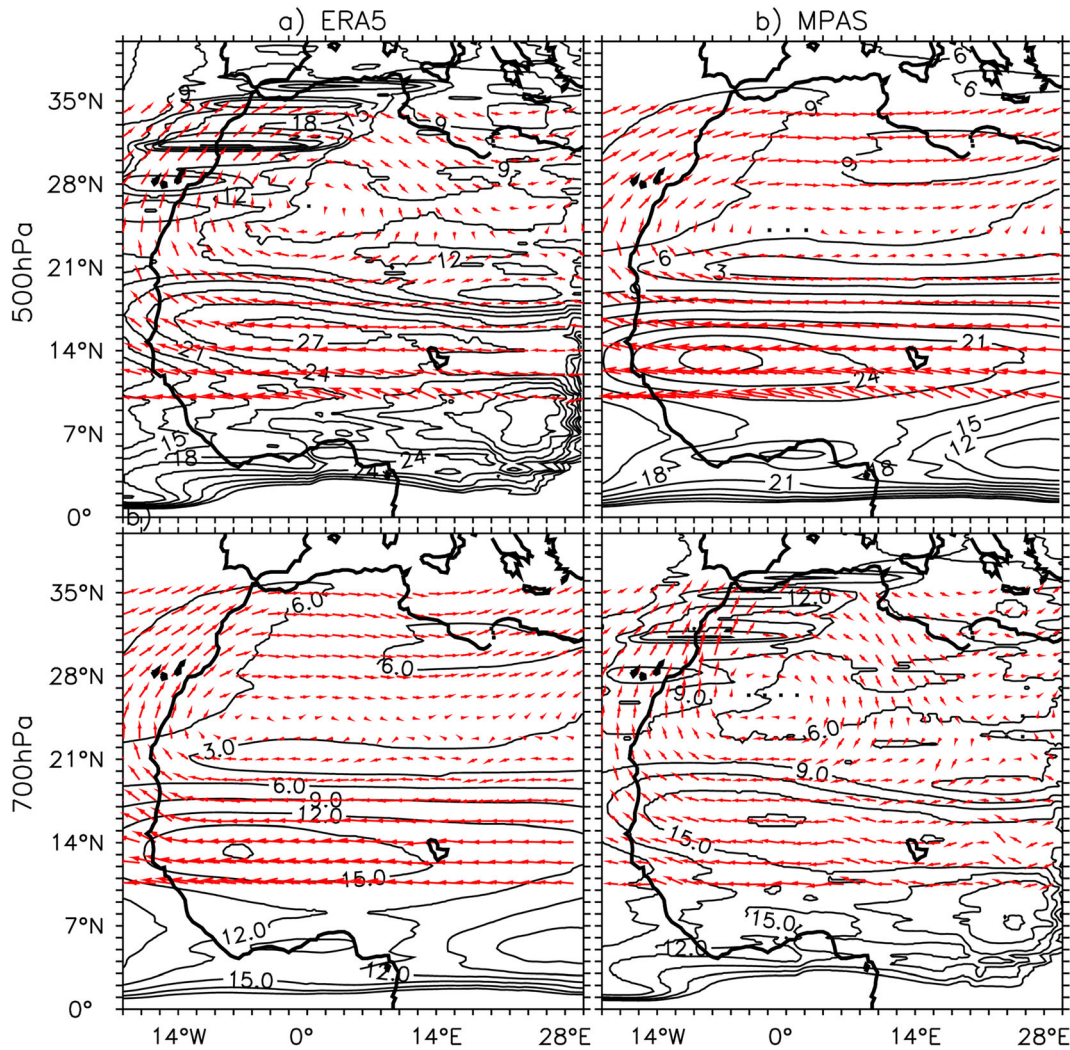


Figure 10. Thermal wind magnitude (contours) and vectors (arrow) for (a) ERA5 and (b) MPAS at 500 and 700 hPa in July.

cause MPAS to simulate a weaker AEJ that may contribute to the dryness in MPAS over the investigated area. This is highlighted in previous studies. For instance, Zhang *et al.* (2021) found that the WAM results from the thermal conditions over the African continent and the neighbouring ocean; therefore, the rainfall variability in a climate model would be actively compatible with the temperature variability.

#### 4. Conclusions

In this study, we investigated the ability of the Model for Prediction Across Scales (MPAS) to simulate the West African Monsoon rainfall and associated atmospheric conditions. The model is initialized using the CSFR reanalysis. Then, we run the model simulation for 30 years, from 1981 to 2010, using a regular grid (uniform resolution of

60 km). The model results are compared with satellite-derived datasets (CHIRPS), gridded observation datasets (CRU), and reanalysed datasets (CSFR, ERA5).

MPAS was able to reproduce the pattern of the annual cycle of the WAM rainfall and the dynamic over West Africa with smaller intensities compared to observed datasets. It also performs better in simulating this cycle than most of the AMIP models used in this study compared to observation data. Additionally, it shows a fine scale of rainfall around the Jos Plateau, in agreement with CHIRPS. MPAS reproduces the seasonal variability of rainfall (in agreement with the observed data), which is characterized by three distinct phases: the monsoon onset and installation phase, the high rain period, and the retreat over the investigated areas. However, MPAS underestimates the rainfall during the peak period over the investigated zones and the orographic zones;

likewise, the magnitude of the vertical velocity and zonal wind are underestimated.

MPAS loses the location of the meridional temperature gradient farther north, as shown by ERA5. In contrast to ERA5, MPAS simulates the temperature gradient at almost the same location in the north for all three summer months (June, July, and August). The misplacement of the gradient in MPAS can influence the atmospheric circulation in the Sahelian zone, as the temperature gradient is responsible for the formation of the jet. Additionally, MPAS simulates smaller areas of thermal wind. This might influence the formation of the wind shear and, hence, the easterly jets; this might cause MPAS to simulate a weaker AEJ, which may contribute to the dryness in MPAS over the investigated area.

In summary, several factors can be linked to the model error leading to the dry bias in the MPAS outputs. These factors include the weak representation of the jets during summer, the weak reproduction of the meridional temperature gradient, and the smaller representation of the thermal activities over the region. All these shortcomings might be influenced by the coarser resolution used in this study. Further study is needed to improve the simulation; for instance, using a variable resolution at finer resolution or SST anomalies may improve the MPAS results obtained from the regular grid.

## Acknowledgements

My sincere appreciation goes to the Federal Ministry of Education and Research (BMBF) and the West African Science Centre on Climate Change and Adapted Land Use (WASCAL) for providing the scholarship and financial support for this programme.

## Author statement

Laouali I Tanimoune carried out the experiment, analysed the data, coordinated this research and drafted the first manuscript. Babatunde J Abiodun supervised and assisted in drafting the manuscript. Nimon Pouwereou assisted in the data analysis. Harald Kunstmann supervised one part of the research and edited the paper. Gerhard Smiatek contributed to the modelling aspect of the paper. Vincent O Ajayi contributed to correcting the

grammatical aspect of the paper. Ibrah S Sanda contributed to the model's setup.

## References

- Abatan A A 2011 *West African extreme daily precipitation in observations and stretched-grid simulations by CAM-EULAG*; Iowa State University.
- Abiodun B J, Pal J S, Afiesimama E A, Gutowski W J and Adedoyin A 2010 Modelling the impacts of deforestation on monsoon rainfall in West Africa; In: IOP Conference Series: Earth and Environmental Science; *IOP Publishing* **13(1)** 012008.
- Abiodun B J, Gutowski W J, Abatan A A and Prusa J M 2011 CAM-EULAG: A non-hydrostatic atmospheric climate model with grid stretching; *Acta Geophys.* **59(6)** 1158–1167.
- Afiesimama E A, Pal J S, Abiodun B J, Gutowski W J and Adedoyin A 2006 Simulation of West African monsoon using the RegCM3. Part I: Model validation and interannual variability; *Theor. Appl. Climatol.* **86(1)** 23–37.
- Ajibola F O, Zhou B, Tchalim Gnitou G and Onyejuruwa A 2020 Evaluation of the performance of CMIP6 HighResMIP on West African precipitation; *J. Atmos.* **11(10)** 1053.
- Akinsanola A A, Ogunjobi K O, Ajayi V O, Adefisan E A, Omotosho J A and Sanogo S 2017 Comparison of five gridded precipitation products at climatological scales over West Africa; *Meteorol. Atmos. Phys.* **129(6)** 669–689.
- Akinsanola A A, Ajayi V O, Adejare A T, Adeyeri O E, Gbode I E, Ogunjobi K O and Abolude A T 2018 Evaluation of rainfall simulations over West Africa in dynamically downscaled CMIP5 global circulation models; *Theor. Appl. Climatol.* **132(1)** 437–450.
- Browne N A and Sylla M B 2012 Regional climate model sensitivity to domain size for the simulation of the West African summer monsoon rainfall; *Int. J. Geophys.* **2012** 625831.
- Broxton P D, Zeng X, Sulla-Menashe D and Troch P A 2014 A global land cover climatology using MODIS data; *J. Appl. Meteorol. Climatol.* **53(6)** 1593–1605.
- Caniaux G, Giordani H, Redelsperger J L, Guichard F, Key E and Wade M 2011 Coupling between the Atlantic cold tongue and the West African monsoon in boreal spring and summer; *J. Geophys. Res. Oceans* **116(C4)** C04003, <https://doi.org/10.1029/2010JC006570>.
- Chagnaud G, Gallée H, Lebel T, Panthou G and Vischel T 2020 A boundary forcing sensitivity analysis of the West African monsoon simulated by the modele atmospherique regional; *J. Atmos.* **11(2)** 191.
- Chen F, Mitchell K, Schaake J, Xue Y, Pan H L, Koren V, Duan Q Y, Ek M and Betts A 1996 Modeling of land surface evaporation by four schemes and comparison with FIFE observations; *J. Geophys. Res. Atmos.* **101(D3)** 7251–7268.
- Cook K H 1999 Generation of the African easterly jet and its role in determining West African precipitation; *J. Clim.* **12(5)** 1165–1184.
- Cook K H and Vizy E K 2006 Coupled model simulations of the West African monsoon system: Twentieth- and twenty-first-century simulations; *J. Clim.* **19(15)** 3681–3703.



- Danielson J J and Gesch D B 2011 *Global multi-resolution terrain elevation data 2010 (GMTED2010)*; Washington, DC, USA: US Department of the Interior, US Geological Survey, 26p.
- Davis N and Birner T 2016 Climate model biases in the width of the tropical belt; *J. Clim.* **29(5)** 1935–1954.
- Diallo I, Sylla M B, Giorgi F, Gaye A T and Camara M 2012 Multimodel GCM-RCM ensemble-based projections of temperature and precipitation over West Africa for the early 21st century; *Int. J. Geophys.* **2012** 972896.
- Donkin P T and Abiodun B J 2023 Capability and sensitivity of MPAS-A in simulating tropical cyclones over the South-West Indian Ocean; *MESE* **9(1)** 527–542.
- Fox-Rabinovitz M, Côté J, Dugas B, Déqué M and McGregor J L 2006 Variable resolution general circulation models: Stretched-grid model intercomparison project (SGMIP); *J. Geophys. Res. Atmos.* **111(D16)** D16104, <https://doi.org/10.1029/2005JD006520>.
- Fox-Rabinovitz M, Cote J, Dugas B, Deque M, McGregor J L and Belochitski A 2008 Stretched-grid Model Intercomparison Project: Decadal regional climate simulations with enhanced variable and uniform-resolution GCMs; *Meteorol. Atmos. Phys.* **100(1)** 159–178.
- Funk C, Peterson P, Landsfeld M, Pedreros D, Verdin J, Shukla S and Michaelsen J 2015 The climate hazards infrared precipitation with stations a new environmental record for monitoring extremes; *Sci. Data* **2(1)** 1–21.
- Gbode I E, Dudhia J, Ogunjobi K O and Ajayi V O 2019 Sensitivity of different physics schemes in the WRF model during a West African monsoon regime; *Theor. Appl. Climatol.* **136** 733–751.
- Grist J P and Nicholson S E 2001 A study of the dynamic factors influencing the rainfall variability in the West African Sahel; *J. Clim.* **14(7)** 1337–1359.
- Hagos S M and Cook K H 2007 Dynamics of the West African monsoon jump; *J. Clim.* **20(21)** 5264–5284.
- Harris L M, Lin S J and Tu C 2016 High-resolution climate simulations using GFDL HiRAM with a stretched global grid; *J. Clim.* **29(11)** 4293–4314.
- Harris I, Osborn T J, Jones P and Lister D 2020 Version 4 of the CRU TS monthly high-resolution gridded multivariate climate dataset; *Sci. Data* **7(1)** 1–18.
- Heinzeller D, Duda M G and Kunstmann H 2016 Towards convection-resolving, global atmospheric simulations with the Model for Prediction Across Scales (MPAS) v3. 1: An extreme scaling experiment; *Geosci. Model Dev.* **9(1)** 77–110.
- Hersbach H, Bell B, Berrisford P, Hirahara S, Horányi A, Muñoz-Sabater J and Simmons A 2020 The ERA5 global reanalysis; *Quart. J. Roy. Meteorol. Soc.* **146(730)** 1999–2049.
- Hourdin F, Musat I, Guichard F S, Ruti P M, Favot F, Filiberti M A and Gallée H 2010 AMMA-model intercomparison project; *Bull. Am. Meteorol.* **91(1)** 95–104.
- Janicot S 1997 Impact of warm ENSO events on atmospheric circulation and convection over the tropical Atlantic and West Africa; *Ann. Geophys.* **15(4)** 471–475.
- Jones P W 1999 First- and second-order conservative remapping schemes for grids in spherical coordinates; *MWR* **127(9)** 2204–2210.
- Ju L, Ringler T and Gunzburger M 2011 Voronoi tessellations and their application to climate and global modeling; In: *Numerical techniques for global atmospheric models*, Columbia, USA, pp. 313–342.
- Klemp J B and Skamarock W C 2021 Adapting the MPAS dynamical core for applications extending into the thermosphere; *J. Adv. Model. Earth Syst.* **13(9)** e2021MS002499.
- Klutse N A B, Sylla M B, Diallo I, Sarr A, Dosio A, Diedhiou A and Büchner M 2016 Daily characteristics of West African summer monsoon precipitation in CORDEX simulations; *Theor. Appl. Climatol.* **123(1)** 369–386.
- Klutse N A B, Quagraine K A, Nkrumah F, Quagraine K T, Berkoh-Oforiwaa R, Dzrobi J F and Sylla M B 2021 The climatic analysis of summer monsoon extreme precipitation events over West Africa in CMIP6 simulations; *Earth Syst. Environ.* **5(1)** 25–41.
- Kramer M, Heinzeller D, Hartmann H, van den Berg W and Steeneveld G J 2020 Assessment of MPAS variable resolution simulations in the grey-zone of convection against WRF model results and observations: An MPAS feasibility study of three extreme weather events in Europe; *Clim. Dyn.* **55(1–2)** 253–276.
- Krishnamurthy V and Ajayamohan R S 2010 Composite structure of monsoon low pressure systems and its relation to Indian rainfall; *J. Clim.* **23(16)** 4285–4305.
- Landu K, Leung L R, Hagos S, Vinoy V, Rauscher S A, Ringler T and Taylor M 2014 The dependence of ITCZ structure on model resolution and dynamical core in aquaplanet simulations; *J. Clim.* **27(6)** 2375–2385.
- Lui Y S, Tse L K S, Tam C Y, Lau K H and Chen J 2021 Performance of MPAS-A and WRF in predicting and simulating western North Pacific tropical cyclone tracks and intensities; *Theor. Appl. Climatol.* **143(1–2)** 505–520.
- Martini M N, Gustafson Jr W I, O'Brien T A and Ma P L 2015 Evaluation of tropical channel refinement using MPAS: A aquaplanet simulations; *J. Adv. Model. Earth Syst.* **7(3)** 1351–1367.
- Matte D, Laprise R, Thériault J M and Lucas-Picher P 2017 Spatial spin-up of fine scales in a regional climate model simulation driven by low-resolution boundary conditions; *Clim. Dyn.* **49(1)** 563–574.
- Michaelis A C, Lackmann G M and Robinson W A 2019 Evaluation of a unique approach to high-resolution climate modeling using the Model for Prediction Across Scales–Atmosphere (MPAS-A) version 5.1; *Geosci. Model Dev.* **12(8)** 3725–3743.
- Niang C, Mohino E, Gaye A T and Omotosho J B 2017 Impact of the Madden Julian Oscillation on the summer West African monsoon in AMIP simulations; *Clim. Dyn.* **48** 2297–2314.
- Nicholson S E 2009 A revised picture of the structure of the 'monsoon' and land ITCZ over West Africa; *Clim. Dyn.* **32** 1155–1171.
- Nicholson S E 2013 The West African Sahel: A review of recent studies on the rainfall regime and its interannual variability; *Int. Sch. Res. Not.* **2013** 453521.
- Nicholson S E and Grist J P 2003 The seasonal evolution of the atmospheric circulation over West Africa and equatorial Africa; *J. Clim.* **6(7)** 1013–1030.
- Nicholson S E and Webster P J 2007 A physical basis for the interannual variability of rainfall in the Sahel; *Quart. J. Roy. Meteorol. Soc.* **133(629)** 2065–2084.
- Odoulami R C, Abiodun B J and Ajayi A E 2019 Modelling the potential impacts of afforestation on extreme precipitation over West Africa; *Clim. Dyn.* **52(3)** 2185–2198.

- Oguntunde P G, Abiodun B J and Lischeid G 2011 Rainfall trends in Nigeria, 1901–2000; *J. Hydrol.* **411(3–4)** 207–218.
- Omotosho J B and Abiodun B J 2007 A numerical study of moisture build-up and rainfall over West Africa; *Meteorol. Appl.* **14(3)** 209–225.
- Pal J S, Giorgi F, Bi X, Elguindi N, Solmon F, Gao X and Steiner A L 2007 Regional climate modeling for the developing world: The ICTP RegCM3 and RegCNET; *Bull. Am. Meteorol. Soc.* **88(9)** 1395–1410.
- Pilon R, Zhang C and Dudhia J 2016 Roles of deep and shallow convection and microphysics in the MJO simulated by the model for prediction across scales; *J. Geophys. Res. Atmos.* **121(18)** 10,575–10,600.
- Raj J, Bangalath H K and Stenchikov G 2019 West African Monsoon: Current state and future projections in a high-resolution AGCM; *Clim. Dyn.* **52(11)** 6441–6461.
- Saha S, Moorthi S, Wu X, Wang J, Nadiga S, Tripp P, Behringer D, Hou Y T, Chuang H Y, Iredell M, Ek M, Meng J, Yang R, Mendez M P, Van Den Dool H, Zhang Q, Wang W, Chen M and Becker E 2014 The NCEP climate forecast system version 2; *J. Clim.* **27(6)** 2185–2208.
- Sivakumar M V, Collins C, Jay A and Hansen J 2014 *Regional priorities for strengthening climate services for farmers in Africa and South Asia*; CCAFS Working Paper.
- Smith I, Moise A, Katzfey J, Nguyen K and Colman R 2013 Regional-scale rainfall projections: Simulations for the New Guinea region using the CCAM model; *J. Geophys. Res. Atmos.* **118(3)** 1271–1280.
- Sultan B and Janicot S 2003 The West African monsoon dynamics. Part II: The ‘preonset’ and ‘onset’ of the summer monsoon; *J. Clim.* **16(21)** 3407–3427.
- Sylla M B, Gaye A T, Pal J S, Jenkins G S and Bi X Q 2009 High-resolution simulations of West African climate using regional climate model (RegCM3) with different lateral boundary conditions; *Theor. Appl. Climatol.* **98(3)** 293–314.
- Sylla M B, Coppola E, Mariotti L, Giorgi F, Ruti P M, Dell’Aquila A and Bi X 2010 Multiyear simulation of the African climate using a regional climate model (RegCM3) with the high resolution ERA-interim reanalysis; *Clim. Dyn.* **35** 231–247.
- Sylla M B, Gaye A T and Jenkins G S 2012 On the fine-scale topography regulating changes in atmospheric hydrological cycle and extreme rainfall over West Africa in a regional climate model projection; *Int. J. Geophys.* **2012** 981649, <https://doi.org/10.1155/2012/981649>.
- Sylla M B, Giorgi F, Coppola E and Mariotti L 2013 Uncertainties in daily rainfall over Africa: Assessment of gridded observation products and evaluation of a regional climate model simulation; *Int. J. Climatol.* **33(7)** 1805–1817.
- Tamoffo A T, Dosio A, Amekudzi L K and Weber T 2022 Process-oriented evaluation of the West African Monsoon system in CORDEX-CORE regional climate models; *Clim. Dyn.* **60(7–8)** 1–24, <https://doi.org/10.1007/s00382-022-06502-y>.
- Thorncroft C D and Blackburn M 1999 Maintenance of the African easterly jet; *Quart. J. Roy. Meteorol. Soc.* **125(555)** 763–786.
- Thuburn J, Ringler T D, Skamarock W C and Klemp J B 2009 Numerical representation of geostrophic modes on arbitrarily structured C-grids; *J. Comput. Phys.* **228(22)** 8321–8335.
- Vizy E K and Cook K H 2002 Development and application of a mesoscale climate model for the tropics: Influence of sea surface temperature anomalies on the West African monsoon; *J. Geophys. Res. Atmos.* **107(D3)** ACL-2.
- Xue Y, De Sales F, Lau W M, Boone A, Feng J, Dirmeyer P and Wu M L C 2010 Intercomparison and analyses of the climatology of the West African Monsoon in the West African Monsoon Modeling and Evaluation project (WAMME) first model intercomparison experiment; *Clim. Dyn.* **35(1)** 3–27.
- Zhang Q, Berntell E, Li Q and Ljungqvist F C 2021 Understanding the variability of the rainfall dipole in West Africa using the EC-Earth last millennium simulation; *Clim. Dyn.* **57(1)** 93–107.
- Springer Nature or its licensor (e.g. a society or other partner) holds exclusive rights to this article under a publishing agreement with the author(s) or other rightsholder(s); author self-archiving of the accepted manuscript version of this article is solely governed by the terms of such publishing agreement and applicable law.

Corresponding editor: PARTHASARATHI MUKHOPADHYAY